
Relative Wasserstein Angle and the Problem of the W_2 -Nearest Gaussian Distribution

Binshuai Wang¹ Peng Wei²

Abstract

We study the problem of quantifying how far an empirical distribution deviates from Gaussianity under the framework of optimal transport. By exploiting the cone geometry of the relative translation invariant quadratic Wasserstein space, we introduce two novel geometric quantities, the relative Wasserstein angle and the orthogonal projection distance, which provide meaningful measures of non-Gaussianity. We prove that the filling cone generated by any two rays in this space is flat, ensuring that angles, projections, and inner products are rigorously well-defined. This geometric viewpoint recasts Gaussian approximation as a projection problem onto the Gaussian cone and reveals that the commonly used moment-matching Gaussian can *not* be the W_2 -nearest Gaussian for a given empirical distribution. In one dimension, we derive closed-form expressions for the proposed quantities and extend them to several classical distribution families, including uniform, Laplace, and logistic distributions; while in high dimensions, we develop an efficient stochastic manifold optimization algorithm based on a semi-discrete dual formulation. Experiments on synthetic data and real-world feature distributions demonstrate that the relative Wasserstein angle is more robust than the Wasserstein distance and that the proposed nearest Gaussian provides a better approximation than moment matching in the evaluation of Fréchet Inception Distance (FID) scores.

1. Introduction

Gaussian distributions play a fundamental role in many areas of machine learning. A wide range of methods either

¹Department of Computer Science, George Washington University, Washington D.C., USA ²MAE, George Washington University, Washington D.C., USA. Correspondence to: Binshuai Wang <derekwang@gwu.edu>, Peng Wei <pwei@gwu.edu>.

Preprint. February 2, 2026.

assume that the underlying distribution is generated directly or implicitly from Gaussian or use Gaussian distributions as convenient approximations to empirical data (Jaynes, 2003). For example, Gaussian noise is commonly adopted as a prior in generative models, including autoregressive models (Oord et al., 2016), Wasserstein GANs (Arjovsky et al., 2017), diffusion models (DDPMs) (Ho et al., 2020), and flow matching methods (Lipman et al., 2022). Moment-matching Gaussian approximations are also widely used in evaluation metrics such as the Fréchet Inception Distance (FID), which compares datasets through their associated Gaussian statistics (Heusel et al., 2017). In addition, many approximation methods, most notably Gaussian mixture models (GMMs), rely on Gaussian distributions as basic blocks to represent complex real-world distributions.

Despite their widespread use, there is limited theoretical understanding of how well a Gaussian distribution approximates a given empirical distribution (Bobkov & Ledoux, 2019). Although various statistical quantities, such as discrepancies in higher-order moments, can be used to capture deviations from the Gaussian family (Jarque & Bera, 1987; Mardia, 1970), these measures do not provide a unified notion of distance between an empirical distribution and its Gaussian surrogate.

Optimal transport (OT) theory provides a geometrical perspective for quantifying differences between probability distributions (Villani & Society, 2003; Villani, 2009). The Wasserstein distance derived from OT endows the space of all probability distributions with a meaningful geometric structure, allowing distributions to be viewed as points in a metric space and compared by their underlying geometry. Because of its strong theoretical foundations and interpretability, OT has become a powerful tool for analyzing the difference between distributions, even involving different types of probability distributions. From this point, it is naturally leads to the following question:

From the perspective of optimal transport, given a probability distribution μ , to what extent can it be regarded as a Gaussian distribution?

Under the 2-Wasserstein distance, we show that this question can be transformed (reduced) to the problem of finding

the minimal orthogonal projection distance from the distribution μ to the convex cone of Gaussian distributions. This geometric viewpoint naturally leads to two measurements, which we term the *relative quadratic Wasserstein angle* (RW_2 angle) and the orthogonal projection distance, which can fully quantify the degree of non-Gaussianity for the distribution μ . We further demonstrate that both measurements admit closed-form solutions in the one-dimensional case, and can be efficiently computed in the high-dimensional case via dual formulation and manifold optimization.

Contributions. The main contributions of this paper are summarized as follows:

- (a) We establish that the notions of the *relative Wasserstein angle* (the RW_2 angle), the orthogonal projection distance, and the inner product are well-defined in the RW_2 metric space. We further show that these quantities provide principled measures for quantifying deviations from the Gaussian family, as well as from other probability families, including the uniform, Laplace, and logistic distributions.
- (b) For one-dimensional settings, we derive *closed-form* solutions for computing the W_2 -nearest Gaussian distribution, and other distributions, including the uniform, Laplace, and logistic distributions. For high-dimensional settings, we develop an efficient algorithm to compute the RW_2 angle and orthogonal projection distance, based on a dual formulation and Riemannian manifold optimization.
- (c) We show that the moment-matching Gaussian is *not* the W_2 -nearest Gaussian approximation for a non-Gaussian distribution, by using the nonzero orthogonal projection distance. We also found that the W_2 -nearest Gaussian approximation can neither share the same set of eigenvalues nor eigenvectors as the moment-matching Gaussian.
- (d) We find that the relative Wasserstein angle provides a more robust measure of non-Gaussianity than the Wasserstein distance, as it compares *rays* rather than individual *points* in the metric space.
- (e) We show that our proposed method can provide Gaussian surrogates that are more faithful than the moment-matching Gaussian, providing improved approximations of feature distributions from commonly used datasets.

Organization. The remainder of the paper is organized as follows. Section 2 reviews classical results in optimal transport theory, including the RW_2 metric space and the Gaussian convex cone. Section 3 presents the definitions of the filling cone, the angle RW_2 and the orthogonal projection distances, and analyzes the solutions in both one-dimensional and high-dimensional settings. Section 4 provides two numerical experiments for validating our theoretical results.

Notations. Let $\mathcal{P}_p(\mathbb{R}^d)$ denote the set of all probability distributions on \mathbb{R}^d with *finite* p -th order moments. Let $\bar{\mu}$ and Σ_μ be the mean and covariance matrix of empirical distribution μ . We write $[\mu]$ for the translation equivalence class of μ and $RW_p([\mu], [\nu])$ for the relative translation invariant Wasserstein distance. The quotient space $\mathcal{P}_2(\mathbb{R}^d)/\sim_T$ is equipped with the RW_2 metric, and $\|[\mu]\|_{RW_2}$ denotes the distance to the apex. Rays induced by dilations are denoted by $[[\mu]] := \{(s \text{Id})_\#[\mu] : s > 0\}$. The relative Wasserstein angle between rays $[[\mu]]$ and $[[\nu]]$ is $\angle([[\mu]], [[\nu]])$, and $p([\mu], [[\nu]])$ denotes the orthogonal projection distance. $\mathcal{N}(0, \Sigma)$ denotes a zero-mean Gaussian with covariance Σ , and $C(\mathcal{N}) := \{\mathcal{N}(0, \Sigma) : \Sigma \succeq 0\}$ denotes the Gaussian cone. The moment-matching Gaussian of μ is $\mathcal{N}(\bar{\mu}, \Sigma_\mu)$. $\hat{\nabla}$ stands for stochastic gradient.

Related Work Quantifying deviation from Gaussianity has a long history in statistics and information theory. Classical approaches rely on higher-order moments, such as skewness and kurtosis, to detect asymmetry and tail behavior beyond the Gaussian model (Mardia, 1970; Jarque & Bera, 1987; D’Agostino & Stephens, 1990). Beyond moment-based criteria, information-theoretic measures characterize non-Gaussianity through entropy and divergence. Representative examples include negentropy (Hyvärinen & Oja, 2000), which exploits the maximum-entropy property of Gaussian distributions, as well as divergence-based measures such as the Kullback–Leibler divergence (Kullback & Leibler, 1951), Rényi divergences, and related quantities in information geometry (Amari, 2016). While powerful and widely used, these approaches are typically tied to specific functionals of the distribution, do not induce a metric structure on the space of probability measures, and do not provide a unified geometric notion of distance for different types of distributions.

Optimal transport offers a different perspective by endowing the space of probability measures with a rich metric geometry via the Wasserstein distance (Villani & Society, 2003; Villani, 2009; Santambrogio, 2015). A number of works have studied Wasserstein distances between general distributions and Gaussian measures, often emphasizing covariance structure or moment-based bounds (Bobkov & Ledoux, 2019; Gelbrich, 1990). Related lines of work investigate Gaussian barycenters and approximations in Wasserstein space (Aguech & Carlier, 2011; Peyré & Cuturi, 2019), as well as scalable variants such as sliced and projected Wasserstein distances (Rabin et al., 2011; Bonneel et al., 2015; Genevay et al., 2019; Feydy et al., 2019). Despite these advances, it is commonly assumed that the moment-matching Gaussian provides a natural Wasserstein approximation for a non-Gaussian distribution. To the best of our knowledge, there has been no prior work demonstrating that this assumption can fail.

2. Preliminaries

2.1. Optimal Transport Theory

Optimal transport theory studies how to transport one probability distribution to another in the least-cost way, given a specified cost function for moving probability mass across a metric space. Formally, given a cost function $c(x, y)$ and two probability measures $\mu(x)$ and $\nu(y)$, the goal is to find a joint distribution (or transport plan) $\gamma(x, y)$ that minimizes the total cost of transporting μ to ν under $c(x, y)$. A common and natural choice for the cost function is a metric-based function of form $c(x, y) = \|x - y\|^p$, where $\|\cdot\|$ is a metric and $p \in [1, \infty)$ (Villani & Society, 2003).

Let μ denote the source distribution and ν the target distribution, with $\mu, \nu \in \mathcal{P}_p(\mathbb{R}^d)$. The p -norm optimal transport problem is defined as follows.

Definition 2.1 (p -norm Optimal Transport Problem (Villani & Society, 2003)).

$$\text{OT}(\mu, \nu, p) := \min_{\gamma \in \Gamma(\mu, \nu)} \int \|x - y\|^p d\gamma(x, y), \quad (1)$$

where $\Gamma(\mu, \nu) = \left\{ \gamma \in \mathcal{P}_p(\mathbb{R}^{2d}) \mid \gamma \geq 0, \int \gamma(x, y) dy = \mu(x), \int \gamma(x, y) dx = \nu(y) \right\}$.

Here, $\gamma(x, y)$ represents a feasible transport plan describing how probability mass is moved from locations x to y . The objective seeks the coupling that minimizes the total transport cost.

This formulation naturally induces a metric on the space of probability distributions, known as the Wasserstein distance (Villani, 2009).

Definition 2.2 (Wasserstein Distance (Villani, 2009)). The p -Wasserstein distance between μ and ν is defined as

$$W_p(\mu, \nu) := \text{OT}(\mu, \nu, p)^{1/p}, \quad p \in [1, \infty).$$

Building upon the p -norm optimal transport problem and the Wasserstein distance, Wang et al. (2024) introduced a translation invariant extension by defining an equivalence relation \sim_T under translations. They showed that the following distance is a well-defined metric on the quotient space $\mathcal{P}_p(\mathbb{R}^d) / \sim_T$.

Definition 2.3 (Relative Translation Invariant Wasserstein Distance). The p th order distance between μ and ν is defined as

$$RW_p([\mu], [\nu]) := \min_{t \in \mathbb{R}^d} \text{OT}(\mu + t, \nu, p)^{1/p},$$

where $[\mu]$ and $[\nu]$ denote the equivalence classes of μ and ν under the translation relation \sim_T .

In the special case $p = 2$, the Wasserstein distance admits the following decomposition:

$$W_2^2(\mu, \nu) = \|\bar{\mu} - \bar{\nu}\|_2^2 + RW_2^2([\mu], [\nu]), \quad (2)$$

where $\bar{\mu}$ and $\bar{\nu}$ denote the means of μ and ν , respectively.

This decomposition shows that the Wasserstein distance naturally can be divided into two components: the first term captures the differences in means, while the second term $RW_2^2([\mu], [\nu])$ measures the internal differences, such as variance and higher-order geometry.

2.2. The Gaussian Convex Cone in the RW_2 Space

Takatsu (2011) showed that the metric completion of all zero-mean Gaussian distributions in the quadratic Wasserstein space $(\mathcal{P}_2(\mathbb{R}^d), W_2)$ naturally forms a *convex cone*,

$$C(\mathcal{N}) = \{ \mathcal{N}(0, \Sigma) \mid \Sigma \in \text{Sym}_*^d \},$$

where Sym_*^d denotes the set of symmetric *nonnegative* semidefinite $d \times d$ covariance matrices.

In this geometry, scaling the covariance matrix corresponds to a geodesic dilation in the W_2 space. Specifically, for any $\Sigma \in \text{Sym}_*^d$ and $s > 0$,

$$\mathcal{N}(0, s^2 \Sigma) = (s \text{Id})_{\#} \mathcal{N}(0, \Sigma),$$

where $(s \text{Id})_{\#}$ denotes the pushforward induced by the scaling map $x \mapsto sx$.

The apex of the convex cone is given by the Dirac measure δ_0 , which corresponds to a degenerate Gaussian distribution with zero covariance. For a fixed covariance matrix Σ , the family

$$\{ \mathcal{N}(0, s^2 \Sigma) : s > 0 \}$$

forms a one-dimensional geodesic ray emanating from the apex, where the matrix Σ encodes the intrinsic *shape* of the Gaussian distribution and the scale parameter s determines its distance from the apex. Distinct covariance matrices generate distinct rays, and all rays constitutes a solid convex cone in the Wasserstein space $(\mathcal{P}_2(\mathbb{R}^d), W_2)$.

3. Methodology

In this section, we develop the main theoretical results of the paper. We first introduce the cone geometry of the RW_2 metric space and define the *relative Wasserstein angle* (the RW_2 angle). By showing that the filling cone between two rays has zero sectional curvature, we establish that orthogonal projections and inner products are also well-defined. We then show that both the RW_2 angle and the projection distance can be used to quantify the degree of non-Gaussianity and find the optimal Gaussian approximations. Finally, we present two algorithms for compute the RW_2 angle and the projection distance for both one-dimensional and high-dimensional settings.

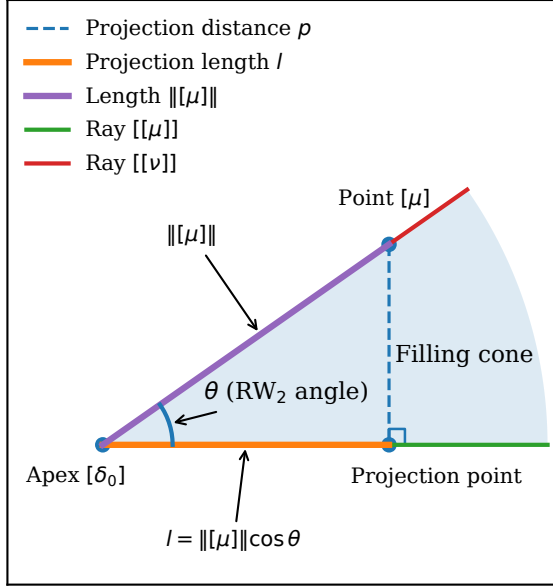


Figure 1. Schematic illustration of the cone geometry in the RW_2 space. The apex $[\delta_0]$ represents the Dirac measure and the rays $[[\mu]]$ and $[[\nu]]$ emanate from this point. The shaded blue region between the two rays is the *filling cone*. The angle θ between the rays corresponds to the relative Wasserstein angle. The point $[\mu]$ lies on the ray $[[\mu]]$ at distance $\|[\mu]\|$ from the apex, and its orthogonal projection onto the ray $[[\mu]]$ has length $l = \|[\mu]\| \cos \theta$.

3.1. RW_2 Angles and Projections

Cone Geometry As noted above, the RW_2 distance defines a genuine metric and therefore induces a metric space $(\mathcal{P}_2(\mathbb{R}^d)/\sim_T, RW_2)$. In contrast to the classical Wasserstein space $(\mathcal{P}_2(\mathbb{R}^d), W_2)$, a distinctive structural feature of $(\mathcal{P}_2(\mathbb{R}^d)/\sim_T, RW_2)$ is its cone geometry. Specifically, all singleton distributions in $(\mathcal{P}_2(\mathbb{R}^d), W_2)$ collapse into the equivalence class $[\delta_0]$, which serves as the *apex* of the space $(\mathcal{P}_2(\mathbb{R}^d)/\sim_T, RW_2)$. All remaining points emanate from this apex and form a family of *rays* generated by different distributional shapes.

To formalize this structure, we introduce the *dilation relation* \sim_S on $(\mathcal{P}_2(\mathbb{R}^d)/\sim_T, RW_2)$, defined by

$$[\mu] \sim_S [\nu] \iff [\nu] = (s \text{Id})_{\#} [\mu], \quad s > 0.$$

Under the dilation relation, the metric space $(\mathcal{P}_2(\mathbb{R}^d)/\sim_T, RW_2)$ excluding the apex can be partitioned into disjoint rays, each of the form

$$\text{ray } [[\mu]] := \{ (s \text{Id})_{\#} [\mu] : s > 0 \},$$

which consist of all distributions that are rescalings of one another. Here, the double-bracket notation $[[\cdot]]$ denotes rays in $(\mathcal{P}_2(\mathbb{R}^d)/\sim_T, RW_2)$, reflecting the fact that rays are induced by both translation and dilation.

Geometrically, each ray $[[\mu]]$ forms a *geodesic line* with respect to the RW_2 metric, since the optimal transport between any two points on the same ray follows the shortest path. Consequently, the space $(\mathcal{P}_2(\mathbb{R}^d)/\sim_T, RW_2)$ admits a cone structure over the space with apex and rays generated by dilations.

Relative Wasserstein Angle Motivated by the theory of angles in metric spaces (Ambrosio et al., 2005), we introduce an angle concept on this quotient space.

Definition 3.1 (Relative Wasserstein Angle). For any two rays $[[\mu]], [[\nu]] \in \mathcal{P}_2(\mathbb{R}^d)/\sim_T$, the *relative Wasserstein angle* between them, denoted by RW_2 angle, is defined by

$$\angle([[\mu]], [[\nu]]) := \arccos \frac{a^2 + b^2 - c^2}{2ab}, \quad (3)$$

where $a = RW_2([\mu], [\delta_0])$, $b = RW_2([\nu], [\delta_0])$, and $c = RW_2([\mu], [\nu])$.

This definition follows the law of cosines and yields a well-defined notion of angle between rays in $(\mathcal{P}_2(\mathbb{R}^d)/\sim_T, RW_2)$. The resulting angle quantifies the *directional* difference between two rays and is invariant under positive rescaling along each ray.

The RW_2 angle can be understood as a rotational difference between two distributions. In particular, when the rays $[[\mu]]$ and $[[\nu]]$ are generated by the identical distribution and differ only by a small rotation, the RW_2 angle coincides with the underlying rotation angle. Moreover, when the rays $[[\mu]]$ and $[[\nu]]$ are generated by different distributions, even if their types are different, this angle is still well-defined.

Orthogonal Projection The classical Wasserstein space is known to be an Alexandrov space with *nonnegative* curvature, in which Euclidean geometric properties do not hold globally in general (Ambrosio et al., 2005; Takatsu, 2011). However, we show that the relative Wasserstein angle behaves like a Euclidean angle, as it can be embedded in a two-dimensional Euclidean plane.

Given any two rays in the RW_2 space, we define the *filling cone* between them as the set of all points lying on geodesics connecting points on the two rays, as is shown in Figure 1. The geometry of this filling cone is characterized by the following result.

Theorem 3.2. *If one of the rays is generated by an absolutely continuous distribution, then the associated filling cone has zero sectional curvature. Moreover, the filling cone is isometric to that of a cone region in the two-dimensional Euclidean plane.*

The proof is provided in Appendix A. This isometric structure of the filling cone allows Euclidean notions, such as

angles and orthogonal projections, to be well-defined in an analogous manner.

Definition 3.3 (Projection Distance). Given a point $[\mu]$ and a ray $[[\nu]]$, the *projection distance* between point $[\mu]$ and ray $[[\nu]]$ is defined by

$$p([\mu], [[\nu]]) := \|[\mu]\|_{RW_2} \sin \angle([\mu], [\nu]). \quad (4)$$

Here $\|[\mu]\|_{RW_2} = RW_2([\mu], [\delta_0])$, serving as the length of the point $[\mu]$ measured from the apex.

We may further define an inner product by $\langle [\mu], [\nu] \rangle = \|[\mu]\|_{RW_2} \|[\nu]\|_{RW_2} \cos \angle([\mu], [\nu])$. This construction can be interpreted as integrating the inner products associated with the corresponding optimal couplings. Nevertheless, the resulting space does not form a vector space, as its underlying geometry is conic rather than linear.

Finally, we emphasize that this structure can not be trivially generalized to cases involving more than two rays. In particular, example E in the Appendix shows the filling cone generated by three rays is not isometric to a cone in three dimensional Euclidean space.

3.2. W_2 -Minimal Gaussian Distribution

We now focus on the central problem: given an empirical distribution μ , to what extent can it be regarded as Gaussian?

From the perspective of optimal transport, this problem can be interpreted geometrically as finding the *minimal W_2 distance* between the given distribution μ and the family of Gaussian distributions. Because of the decomposition in Equation 2, the mean of any Gaussian minimizer must coincide with the mean of μ . Consequently, the problem can be reduced to optimizing over the covariance matrices of Gaussian distributions.

Projection onto the Gaussian Cone. As mentioned above, the set of all Gaussian distributions forms a convex cone $C(\mathcal{N})$ in the RW_2 metric space. This Gaussian cone consists of a single apex together with a family of disjoint Gaussian rays differing by their covariances. As the minimal W_2 distance must be a projection distance from the point $[\mu]$ to a certain ray within the Gaussian cone $C(\mathcal{N})$, the problem of finding the minimal W_2 distance from distribution μ to a Gaussian distribution is equivalent to finding the projection distance from the point $[\mu]$ onto the Gaussian cone $C(\mathcal{N})$ in the metric space $(\mathcal{P}_2(\mathbb{R}^d)/\sim_T, RW_2)$. Moreover, since projection distances in this space are characterized by angles, this problem can equivalently be viewed as finding the minimal relative Wasserstein angle between the ray $[\mu]$ and a Gaussian ray.

In particular, if μ itself is Gaussian, the ray $[[\mu]]$ coincides with a Gaussian ray, and both the projection distance and the

RW_2 angle are zero. In contrast, when μ is non-Gaussian, the projection distance and the corresponding RW_2 angle are strictly positive. As a result, both the projection and the angle can quantify the degree of non-Gaussianity of the distribution μ .

Solutions. In the one-dimensional setting, the problem admits a closed-form solution for distribution μ . In this case, both the RW_2 angle and the projection distance can fully quantify the non-Gaussianity; detailed results are presented in Subsection 3.3.

In contrast, in high-dimensional settings, the optimal transport problem generally does not admit an analytical solution, except for distributions with special structures (e.g., coordinate-separable distributions in a PCA basis; see Section D). We therefore resort to numerical methods to solve the problem, which are discussed in detail in Subsection 3.4.

The Moment-Matching Gaussian. A commonly used Gaussian approximation of μ in statistics is the moment-matching Gaussian distribution $\mathcal{N}(\bar{\mu}, \Sigma_\mu)$, where $\bar{\mu}$ and Σ_μ denote the mean and covariance of μ , respectively. It is natural to conjecture that this distribution is also the W_2 -nearest Gaussian to μ . However, we show that when μ is non-Gaussian, the moment-matching Gaussian can *not* be the optimal solution under the RW_2 metric.

To see this, observe that when μ is non-Gaussian, the moment-matching Gaussian shares the same covariance matrix as μ , and hence has the same length $\|[\mu]\|_{RW_2}$. Nevertheless, the projection point of $[\mu]$ onto the Gaussian ray is different from the moment-matching Gaussian, as the length of the projection point is smaller than $\|[\mu]\|_{RW_2}$. This implies that the moment-matching Gaussian can not be the nearest Gaussian approximation of μ .

Moreover, we demonstrate that for certain distribution μ , the nearest Gaussian distribution may neither share the same eigenvalues nor eigenvectors of the covariance matrix (one illustrative example is provided in Appendix F). This example suggests that analytic solutions are unlikely to exist in general for high-dimensional cases. Therefore, we adopt computational approaches based on dual formulation and manifold optimization, which are described in Subsection 3.4.

3.3. Closed-Form Solution in One Dimension

Let μ be a discrete probability distribution on \mathbb{R} with zero mean,

$$\mu := \frac{1}{n} \sum_{i=1}^n \delta_{x_i}, \quad \bar{\mu} = 0,$$

where $x_1 \leq \dots \leq x_n$ are real-valued samples, assumed to be sorted in ascending order.

We consider the family of Gaussian distributions $\mathcal{N}(0, \sigma^2)$ with $\sigma \geq 0$. Let ϕ and Φ denote the probability density function (PDF) and cumulative distribution function (CDF) of the standard normal distribution $\mathcal{N}(0, 1)$, respectively, and define

$$\sigma_\mu := \sqrt{\frac{1}{n} \sum_{i=1}^n x_i^2}, \quad z_i := \Phi^{-1}\left(\frac{i}{n}\right),$$

where $z_0 := -\infty$, $z_n := +\infty$.

Proposition 3.4 (Closed-Form Projection Distance and RW_2 Angle in One Dimension). *Let μ be a one-dimensional empirical distribution with zero mean as above. Then the relative Wasserstein angle θ and the projection distance p of the point $[\mu]$ onto the Gaussian ray $[[\mathcal{N}(0, \sigma^2)]]$ are given by*

$$\theta = \arccos\left(\frac{l}{\sigma_\mu}\right), \quad p = \sigma_\mu \sin \theta, \quad (5)$$

where $l = \sum_{i=1}^n x_i(\phi(z_{i-1}) - \phi(z_i))$.

Both the relative Wasserstein angle θ and the projection distance p depend solely on the empirical distribution μ and are independent of the Gaussian scale parameter σ . A detailed derivation of Proposition 3.4 is provided in Appendix B. Algorithm 1 summarizes the procedure for computing the projection distance and the RW_2 angle in one dimension.

Algorithm 1 Projection Distance and RW_2 Angle (1D)

Require: Samples $\{x_i\}_{i=1}^n \subset \mathbb{R}$
Ensure: Projection distance p and RW_2 angle θ

- 1: Center data: $x_i \leftarrow x_i - \frac{1}{n} \sum_j x_j$
- 2: Sort $x_1 \leq \dots \leq x_n$
- 3: $\sigma_\mu \leftarrow \sqrt{\frac{1}{n} \sum_i x_i^2}$
- 4: $z_i \leftarrow \Phi^{-1}\left(\frac{i}{n}\right)$, $z_0 = -\infty$, $z_n = +\infty$
- 5: $l \leftarrow \sum_{i=1}^n x_i(\phi(z_{i-1}) - \phi(z_i))$
- 6: $\theta \leftarrow \arccos\left(\frac{l}{\sigma_\mu}\right)$
- 7: $p \leftarrow \sigma_\mu \sin \theta$

output p, θ

Complexity. The algorithm runs in $\mathcal{O}(n \log n)$ time due to sorting and requires $\mathcal{O}(n)$ memory.

Discussion. Equation (5) also appeared in the literature (Brown & Hettmansperger, 1996; Cuesta-Albertos et al., 1999), although these works do not derive the formula from the geometric perspective of angles and orthogonal projections in the metric space.

The same approach can be extended to other classes of distributions parametrized by mean and scale, such as uniform,

Laplace, and logistic distributions; the exact formulae are provided in Appendix C. For distribution families that are not parametrized solely by mean and scale, the problem corresponds to projecting onto more general curves in the RW_2 space, which we leave for future investigation.

3.4. Solution in High Dimensions

In low dimensions, the RW_2 distance can be computed using power diagram methods or discrete optimal transport solvers (Peyré & Cuturi, 2019). However, these approaches become impractical in high dimensions due to the complexity of Laguerre cells and the curse of dimensionality. To overcome this difficulty, we combine a semi-discrete dual formulation of the RW_2 distance with stochastic Riemannian optimization over the Gaussian covariances.

We decompose the high-dimensional procedure into two components: 1) evaluation of $RW_2(\mu, \mathcal{N}(0, \Sigma))$ via a dual formulation; 2) optimization over Gaussian covariances using manifold optimization to identify the nearest Gaussian. Due to space limitations, the first component is described to Appendix H, while we focus on the second component.

3.4.1. MANIFOLD OPTIMIZATION FOR GAUSSIAN COVARIANCES

Using the eigendecomposition, we parameterize the Gaussian covariance as

$$\Sigma = R \Lambda R^\top, R^\top R = I, \Lambda = \text{diag}(\lambda), \lambda \geq 0, \mathbf{1}^\top \lambda \leq 1.$$

The trace constraint $\mathbf{1}^\top \lambda \leq 1$ follows from the fact that both the empirical distribution and candidate Gaussian distributions can be restricted in the unit ball of the RW_2 space.

Under this parameterization, the covariance optimization problem can be optimized by using stochastic Riemannian optimization, as summarized in Algorithm 2.

Algorithm 2 Nearest Gaussian in High-Dim Case

Require: Samples $\{x_i\}_{i=1}^n$, dual potential f , outer iterations K_2 ; batch size m_b ; stepsizes η_R, η_Λ .

Ensure: Optimal covariance Σ^* .

- 1: Initialize $R^{(0)}, \lambda^{(0)}$, and $\Lambda^{(0)} = \text{diag}(\lambda^{(0)})$
- 2: **for** $t = 0, \dots, K_2 - 1$ **do**
- 3: Sample $\xi_\ell \sim \mathcal{N}(0, I_d)$ and set $Y_\ell = R^{(t)}(\Lambda^{(t)})^{1/2} \xi_\ell$
- 4: **for** $\ell = 1, \dots, m_b$ **do**
- 5: $i_\ell \in \arg \min_i \left(\frac{1}{2} \|x_i - Y_\ell\|^2 - f_i \right)$
- 6: $r_\ell \leftarrow Y_\ell - x_{i_\ell}$
- 7: **end for**
- 8: Update R via Riemannian descent using $\hat{\nabla}_R L$
- 9: Update λ via projected gradient using $\hat{\nabla}_\lambda L$
- 10: $\Sigma^{(t+1)} \leftarrow R \Lambda R^\top$
- 11: **end for**

output $\Sigma^* = \Sigma^{(T)}$

Stochastic Gradient Formulas. Let $\{x_i\}_{i=1}^n$ be the samples from the empirical distribution μ and $\{\xi_\ell\}_{i=1}^{m_b}$ be the samples from $\mathcal{N}(0, I_d)$, where n is the number of samples and m_b is the batchsize in the dual form. Let $Y_\ell = R\Lambda^{1/2}\xi_\ell$ and $r_\ell = Y_\ell - x_\ell$. The stochastic gradients are given by

$$\hat{\nabla}_R L = \frac{1}{m_b} \sum_{\ell=1}^{m_b} r_\ell (\Lambda^{1/2}\xi_\ell)^\top,$$

$$\hat{\nabla}_\lambda L = \frac{1}{2m_b} \sum_{\ell=1}^{m_b} (R^\top r_\ell) \odot \frac{\xi_\ell}{\sqrt{\lambda}}.$$

3.4.2. ALTERNATING OPTIMIZATION SCHEME

Combining the distance evaluation procedure in Appendix H with the manifold optimization above, we obtain the following alternating scheme for computing the RW_2 -nearest Gaussian distribution.

Algorithm 3 Alternating Scheme in High-Dim Case

Require: Empirical samples $\{x_i\}_{i=1}^n \subset \mathbb{R}^d$ (centered with unit length); outer iterations T ; batch size m ; stepsizes $\eta_f, \eta_R, \eta_\Lambda$.

Ensure: Approximate nearest Gaussian covariance Σ^* , projection distance p^* , and angle θ^* .

- 1: Initialize covariance $\Sigma^{(0)}$ with $\text{tr}(\Sigma^{(0)}) \leq 1$
- 2: **for** $t = 0, 1, \dots, T - 1$ **do**
- 3: **(A) RW_2 distance evaluation:**
- 4: Using Appendix Algorithm 4, compute the dual potential $f^{(t)}$ and $RW_2(\mu, \mathcal{N}(0, \Sigma^{(t)}))$
- 5: **(B) Covariance update:**
- 6: Update $\Sigma^{(t+1)}$ via one Riemannian descent step using $f^{(t)}$ (Algorithm 2)
- 7: **end for**
- 8: Set $\Sigma^* = \Sigma^{(T)}$
- 9: Compute the projection distance p^* and the relative Wasserstein angle θ^*
- output** Σ^*, p^*, θ^*

4. Experiments

In this section, we present two experiments to validate the proposed theory. The first experiment investigates the non-Gaussianity caused by finite-sample effects in a low-dimensional setting, illustrating how the RW_2 angle and the projection distance provide quantitative measures of deviation from Gaussianity for finite samples. The second experiment focuses on the non-Gaussianity of feature distributions of commonly used machine learning datasets in the evaluation of FID scores, and shows our approach can provide a better estimator.

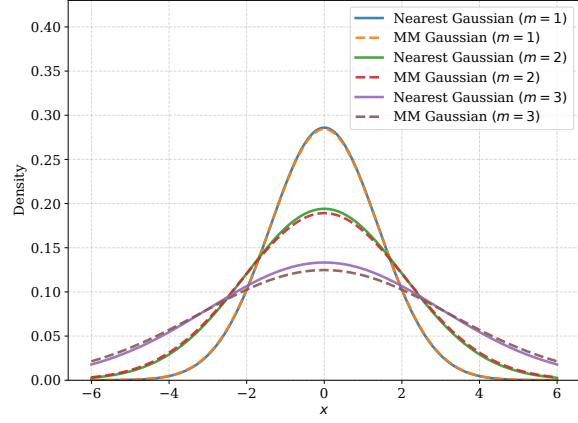
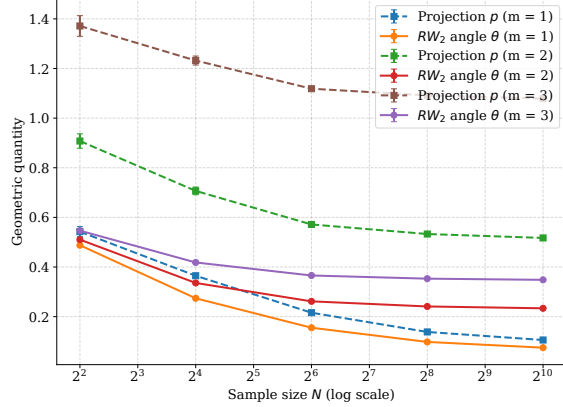


Figure 2. **Top:** Evolution of the RW_2 angle θ and the projection distance p as functions of the sample size N . Shaded regions indicate one standard deviation over repeated experiments. As N increases, both quantities decrease, reflecting the decay of finite-sample non-Gaussianity. **Bottom:** Gaussian approximation at a fixed sample size $N = 64$. For each m , the solid curve represents the RW_2 -nearest Gaussian, and the dashed curve represents the moment-matching Gaussian. Although the two Gaussian approximations are close, they do not coincide, and the difference becomes larger as m increases.

4.1. Finite-Sample Effects in the Low-Dimensional Case

Setup. We construct empirical distributions by sampling $N \in \{2^2, 2^4, 2^6, 2^8, 2^{10}\}$ points from a Gaussian mixture model with two equally weighted components, $\mathcal{N}(-m, 1)$ and $\mathcal{N}(m, 1)$. The parameter m controls the separation between the two component means and is chosen from $\{1, 2, 3\}$. The target distribution is the standard Gaussian $\mathcal{N}(0, 1)$. For each sample size N , we compute the corresponding RW_2 angle θ and projection distance p between the finite samples and the Gaussian ray. All quantities are averaged over 10 independent repetitions, and the associated variances are reported for sampling variability.

Results. Figure 2 (Top) shows that, as the sample size N increases, both the RW_2 angle θ and the projection distance

p decrease monotonically. For fixed m , both quantities converge to finite limiting values. These limits correspond to the exact geometric relationship between the underlying Gaussian mixture distribution and the standard Gaussian distribution as $N \rightarrow \infty$. Moreover, larger values of m lead to consistently larger values of θ and p , indicating increasing deviation from Gaussianity as the separation between mixture components grows.

Notably, the projection distance exhibits substantially larger variance across trials than the RW_2 angle, particularly for small sample sizes. This behavior arises because the projection distance measures differences between *points*, whereas the RW_2 angle compares *rays* and is therefore scale-invariant and more robust to finite-sample fluctuations.

The bottom panel of Figure 2 provides a concrete illustration for $N = 64$, confirming that the moment-matching Gaussian is close but not identical to the RW_2 -nearest Gaussian.

4.2. Evaluation on Non-Gaussianity of Feature Distributions

Setup. We evaluate the non-Gaussianity of feature distributions arising from commonly used benchmarks in generative modeling, including CIFAR-10 (Krizhevsky & Hinton, 2009), MNIST (LeCun et al., 1998), CelebA-64 (Liu et al., 2015), and LSUN (Yu et al., 2015). All experiments are conducted using Algorithm 3, with features extracted from the Inception-V3 network (Szegedy et al., 2016), following standard practice in FID-based evaluations.

For each dataset, we treat the empirical distribution of features extracted from the entire dataset as the source distribution and compute its RW_2 -nearest Gaussian approximation. We compare the relative Wasserstein angle θ^* and projection distance p^* of the nearest Gaussian with the corresponding quantities θ_{MM} and p_{MM} obtained from the moment-matching Gaussian. To mitigate the effects of stochasticity introduced by Monte Carlo sampling and optimization, each experiment is repeated independently 10 times under identical configurations. We report both the mean and variance of both quantities across trials.

Results. Table 1 summarizes the relative Wasserstein angle and projection distance for commonly used datasets' feature distributions. Across all datasets, the W_2 -nearest Gaussian consistently achieves a smaller relative Wasserstein angle than the moment-matching Gaussian. For example, for CIFAR-10, the angle decreases from $\theta_{\text{MM}} \approx 1.12$ to $\theta^* \approx 0.91$, corresponding to a reduction of nearly 12° . In addition, the W_2 -nearest Gaussian also yields a smaller projection distance p^* . These improvements are stable across repeated trials, as reflected by the consistently small variances reported in Table 1. Together, these results demonstrate that moment matching alone can substantially overestimate the

Table 1. Non-Gaussianity of feature distributions measured by the relative Wasserstein angle and projection distance. We report the mean and variance (over 10 trials) of the relative Wasserstein angle θ and projection distance p for the W_2 -nearest Gaussian (RW_2^*) and the moment-matching Gaussian (MM). Variance scales are indicated in the column headers; all values are rounded to two decimal digits.

Dataset / Method	θ (rad) (var $\times 10^{-4}$)	p (var $\times 10^{-5}$)
CIFAR-10 (RW_2^*)	0.92 ± 1.02	0.79 ± 3.70
CIFAR-10 (MM)	1.12 ± 0.01	0.90 ± 0.01
MNIST (RW_2^*)	0.76 ± 0.50	0.69 ± 2.62
MNIST (MM)	0.94 ± 0.01	0.81 ± 0.04
CelebA-64 (RW_2^*)	0.75 ± 1.12	0.68 ± 5.98
CelebA-64 (MM)	0.97 ± 0.01	0.83 ± 0.03
LSUN-Church (RW_2^*)	0.82 ± 0.75	0.73 ± 3.53
LSUN-Church (MM)	1.02 ± 0.01	0.85 ± 0.01

degree of Gaussianity in high-dimensional feature distributions, whereas the proposed RW_2 -nearest provide a more faithful approximation.

5. Conclusion

We proposed a geometric framework for quantifying non-Gaussianity in optimal transport by introducing the relative Wasserstein angle and orthogonal projection distance in the RW_2 space. Exploiting the cone geometry induced by translations and dilations, we showed that the filling cone generated by two rays is flat, which ensures that angles and projections are well-defined.

This viewpoint reframes Gaussian approximation as a projection problem onto the Gaussian cone in Wasserstein space. As a consequence, the commonly used moment-matching Gaussian is generally *not* the W_2 -nearest Gaussian for non-Gaussian distributions, a discrepancy precisely captured by the projection distance and the RW_2 angle.

We derived closed-form solutions in one dimension and developed an efficient stochastic Riemannian optimization method for high-dimensional settings. Experiments on synthetic data and real-world feature distributions demonstrate that the proposed RW_2 -nearest Gaussian provides a closer and more stable approximation than moment matching, particularly in high dimensions.

More broadly, this work shows that angles and projections in Wasserstein geometry offer robust, scale-invariant tools for distribution comparison, with potential applications beyond Gaussian models, including other parametric families and generative model evaluation.

Impact Statement

This paper presents work whose goal is to advance the field of Machine Learning. There are many potential societal consequences of our work; findings from this paper provide a novel in-depth understanding of the properties and limitations of the FID score.

References

Aguech, M. and Carlier, G. Barycenters in the wasserstein space. *SIAM Journal on Mathematical Analysis*, 43(2): 904–924, 2011.

Amari, S. *Information Geometry and Its Applications*, volume 194 of *Applied Mathematical Sciences*. Springer, 2016.

Ambrosio, L., Gigli, N., and Savaré, G. Gradient flows in metric spaces and in the space of probability measures. *Lectures in Mathematics, ETH Zurich*, 2005.

Arjovsky, M., Chintala, S., and Bottou, L. Wasserstein generative adversarial networks. In *Proceedings of the 34th International Conference on Machine Learning*, volume 70, pp. 214–223. PMLR, 2017.

Bobkov, S. G. and Ledoux, M. One-dimensional empirical measures, order statistics, and kantorovich transport distances. *Memoirs of the American Mathematical Society*, 2019.

Bonneel, N., Peyré, G., and Cuturi, M. Sliced and radon wasserstein barycenters of measures. *Journal of Mathematical Imaging and Vision*, 51(1):22–45, 2015.

Brown, B. M. and Hettmansperger, T. P. Normal scores, normal plots tests for normality. *Journal of the American Statistical Association*, 91(436):1668–1675, 1996.

Cuesta-Albertos, J. A., Matrán, C., Rodríguez-Rodríguez, J. M., and del Barrio, E. Tests of goodness of fit based on the l_2 -wasserstein distance. *The Annals of Statistics*, 27 (4):1230 – 1239, 1999.

D’Agostino, R. B. and Stephens, M. A. A suggestion for using powerful and informative tests of normality. *The American Statistician*, 44(4):316–321, 1990.

Feydy, J., Chizat, L., Vialard, F.-X., Amari, S.-i., Peyré, G., and Courty, N. Interpolating between optimal transport and mmd using sinkhorn divergences. *Proceedings of the 22nd International Conference on Artificial Intelligence and Statistics*, 2019.

Gelbrich, M. On a formula for the l^2 wasserstein metric between measures on euclidean and hilbert spaces. *Mathematische Nachrichten*, 147:185–203, 1990.

Genevay, A., Chizat, L., Bach, F., Cuturi, M., and Peyré, G. Sample complexity of sinkhorn divergences. *Proceedings of the 22nd International Conference on Artificial Intelligence and Statistics*, 2019.

Heusel, M., Ramsauer, H., Unterthiner, T., Nessler, B., and Hochreiter, S. GANs trained by a two time-scale update rule converge to a local nash equilibrium. In *Proceedings of the 31st International Conference on Neural Information Processing Systems (NeurIPS)*, pp. 6629–6640, Long Beach, CA, USA, 2017.

Ho, J., Jain, A., and Abbeel, P. Denoising diffusion probabilistic models. *arXiv preprint arxiv:2006.11239*, 2020.

Hyvärinen, A. and Oja, E. Independent component analysis: algorithms and applications. *Neural Networks*, 13(4–5): 411–430, 2000.

Jarque, C. M. and Bera, A. K. A test for normality of observations and regression residuals. *International Statistical Review*, 55(2):163–172, 1987.

Jaynes, E. T. *Probability Theory: The Logic of Science*. Cambridge University Press, 2003.

Krizhevsky, A. and Hinton, G. Learning multiple layers of features from tiny images. Technical report, University of Toronto, 2009.

Kullback, S. and Leibler, R. A. On information and sufficiency. *The Annals of Mathematical Statistics*, 22(1): 79–86, 1951.

LeCun, Y., Bottou, L., Bengio, Y., and Haffner, P. Gradient-based learning applied to document recognition. *Proceedings of the IEEE*, 86(11):2278–2324, 1998.

Lipman, Y., Chen, R. T. Q., Ben-Hamu, H., Nickel, M., and Le, M. Flow matching for generative modeling. *ArXiv*, abs/2210.02747, 2022.

Liu, Z., Luo, P., Wang, X., and Tang, X. Deep learning face attributes in the wild. In *Proceedings of the IEEE International Conference on Computer Vision (ICCV)*, 2015.

Mardia, K. V. Measures of multivariate skewness and kurtosis with applications. *Biometrika*, 57(3):519–530, 1970.

Oord, A., Kalchbrenner, N., and Kavukcuoglu, K. Pixel recurrent neural networks. *CoRR*, abs/1601.06759, 2016.

Peyré, G. and Cuturi, M. *Computational Optimal Transport. Foundations and Trends in Machine Learning*, 2019.

Rabin, J., Peyré, G., Delon, J., and Bernot, M. Wasserstein barycenter and its application to texture mixing. In *Scale Space and Variational Methods in Computer Vision*, pp. 435–446, 2011.

Santambrogio, F. *Optimal Transport for Applied Mathematicians*. Birkhäuser, 2015.

Szegedy, C., Vanhoucke, V., Ioffe, S., Shlens, J., and Wojna, Z. Rethinking the inception architecture for computer vision. In *Proceedings of the IEEE Conference on Computer Vision and Pattern Recognition (CVPR)*, 2016.

Takatsu, A. Wasserstein geometry of gaussian measures. *Osaka Journal of Mathematics*, 48(4):1005–1026, 2011.

Villani, C. *Optimal Transport: Old and New*. Springer, 2009.

Villani, C. and Society, A. M. *Topics in Optimal Transportation*. Graduate studies in mathematics. American Mathematical Society, 2003.

Wang, B., Di, Q., Yin, M., Wang, M., Gu, Q., and Wei, P. Relative-translation invariant wasserstein distance, 2024.

Yu, F., Seff, A., Zhang, Y., Song, S., Funkhouser, T., and Xiao, J. Lsun: Construction of a large-scale image dataset using deep learning with humans in the loop. In *Proceedings of the IEEE Conference on Computer Vision and Pattern Recognition (CVPR)*, 2015.

Appendix

A. Proof of Flatness of the Filling Cone

In this section, we prove that the two-dimensional filling cone generated by two rays emanating from the apex $[\delta_0]$ in the quotient space $(\mathcal{P}_2(\mathbb{R}^d)/\sim_T, RW_2)$ is flat whenever one of the rays is generated by an absolutely continuous distribution. The key observation is that, after a unique optimal alignment ensured by Brenier’s theorem, all Wasserstein distances between any pair of points within the filling cone are induced by a fixed quadratic form in a global affine coordinate system.

A.1. Setup and Notation

Let $[\mu], [\nu] \in \mathcal{P}_2(\mathbb{R}^d)/\sim_T$. Without loss of generality, we assume that both representative elements are centered and normalized to unit RW_2 norm, i.e.,

$$\bar{\mu} = \bar{\nu} = 0, \quad \|\mu\|_{RW_2} = \|\nu\|_{RW_2} = 1.$$

Throughout the proof, we assume that μ is absolutely continuous.

A.2. Uniqueness of the Aligned Optimal Map

Lemma A.1 (Uniqueness of the Optimal Transport Map). *If μ is absolutely continuous, then the optimal transport plan between μ and ν for the quadratic cost is unique and given by $(\text{Id}, T)_{\#}\mu$, where $T = \nabla\phi$ is the gradient of a convex function.*

Proof. This is a direct consequence of Brenier’s theorem for the quadratic cost. \square

A.3. Geodesics in the Filling Cone

Lemma A.2 (Form of Geodesics). *For any $s_0, s_1 \geq 0$, the W_2 -geodesic between*

$$\rho_0 := (s_0 \text{Id})_{\#}\mu, \quad \rho_1 := (s_1 T)_{\#}\mu$$

is given by

$$\rho_t = (F_t)_{\#}\mu, \quad F_t(x) := (1-t)s_0 x + t s_1 T(x), \quad t \in [0, 1].$$

Proof. This follows from McCann’s displacement interpolation, generated by the unique optimal plan $(\text{Id}, T)_{\#}\mu$, composed with the endpoint scalings $x \mapsto s_0 x$ and $y \mapsto s_1 y$. The result also extends trivially to the cases where $s_0 = 0$ or $s_1 = 0$. \square

Thus, every point on the geodesic can be written in the affine form

$$F_t(x) = ax + bT(x), \quad (a, b) = ((1-t)s_0, ts_1) \in \mathbb{R}_{\geq 0}^2.$$

This provides a global affine coordinate chart on the filling cone.

For general $a, b \geq 0$, define

$$S_{a,b}(x) := a x + b T(x), \quad \rho_{a,b} := (S_{a,b})_{\#} \mu.$$

The filling cone is precisely the image of the map

$$\Phi : \mathbb{R}_{\geq 0}^2 \rightarrow \mathcal{P}_2(\mathbb{R}^d)/\sim_T, \quad \Phi(a, b) = \rho_{a,b}.$$

A.4. Exact W_2 Distances inside the Filling Cone

Lemma A.3 (Exact Distance Formula). *For any $(a_1, b_1), (a_2, b_2) \in \mathbb{R}_{\geq 0}^2$,*

$$W_2^2(\rho_{a_1, b_1}, \rho_{a_2, b_2}) = \int_{\mathbb{R}^d} \|(a_1 - a_2)x + (b_1 - b_2)T(x)\|^2 d\mu.$$

Proof. Consider the transport plan

$$\pi := (S_{a_1, b_1}, S_{a_2, b_2})_{\#} \mu.$$

We show that π is the optimal plan by using the cyclic inequality

$$\sum_{i=1}^m \langle x_{i+1}, y_{i+1} - y_i \rangle \geq 0,$$

where $x_{m+1} = x_1, y_{m+1} = y_1$.

Let $\Gamma = \{(x, T(x))\}$ be the support of $(\text{Id}, T)_{\#} \mu$. Since Γ is c -cyclically monotone,

$$\Sigma_{xy} := \sum_i \langle x_{i+1}, T(x_{i+1}) - T(x_i) \rangle \geq 0.$$

Because the quadratic cost is symmetric, the flipped graph $\Gamma^{\top} = \{(T(x), x)\}$ is also c -cyclically monotone, giving

$$\Sigma_{yx} := \sum_i \langle T(x_{i+1}), x_{i+1} - x_i \rangle \geq 0.$$

Set $y_i := T(x_i)$ and define

$$\begin{aligned} u_i &:= S_{a_1, b_1}(x_i) = a_1 x_i + b_1 y_i, \\ v_i &:= S_{a_2, b_2}(x_i) = a_2 x_i + b_2 y_i. \end{aligned}$$

Then

$$\begin{aligned} \sum_i \langle u_{i+1}, v_{i+1} - v_i \rangle &= a_1 a_2 \Sigma_{xx} + a_1 b_2 \Sigma_{xy} \\ &\quad + b_1 a_2 \Sigma_{yx} + b_1 b_2 \Sigma_{yy}. \end{aligned}$$

where

$$\Sigma_{xx} := \sum_i \langle x_{i+1}, x_{i+1} - x_i \rangle,$$

$$\Sigma_{yy} := \sum_i \langle y_{i+1}, y_{i+1} - y_i \rangle.$$

A telescoping identity gives $\Sigma_{zz} = \frac{1}{2} \sum_i \|z_{i+1} - z_i\|^2 \geq 0$ for $z = x, y$. Thus every Σ term is nonnegative, and since $a_j, b_j \geq 0$, we conclude

$$\sum_i \langle u_{i+1}, v_{i+1} - v_i \rangle \geq 0.$$

Hence the support of π is c -cyclically monotone. By the standard characterization of optimal transport for the quadratic cost, π is optimal, and its cost equals $W_2^2(\rho_{a_1, b_1}, \rho_{a_2, b_2})$, yielding the desired expression. \square

A.5. Flatness of the Filling Cone

Quadratic form. Expanding the square in Lemma A.3,

$$\begin{aligned} W_2^2(\rho_{a_1, b_1}, \rho_{a_2, b_2}) &= (a_1 - a_2)^2 A + (b_1 - b_2)^2 C \\ &\quad + 2(a_1 - a_2)(b_1 - b_2)B. \end{aligned}$$

where $A = \int \|x\|^2 d\mu$, $B = \int \langle x, T(x) \rangle d\mu$, $C = \int \|T(x)\|^2 d\mu$.

These constants depend only on (μ, T) .

Proposition A.4 (Flatness of the Filling Cone). *The pull-back of the W_2 -metric under $\Phi(a, b) = (S_{a,b})_{\#} \mu$ is the constant bilinear form*

$$g = \begin{pmatrix} A & B \\ B & C \end{pmatrix}$$

in the global affine coordinates (a, b) . Consequently, the induced two-dimensional Riemannian manifold is flat, with zero Gaussian curvature.

Proof. Lemma A.3 shows that squared distances depend only on the differences $(a_1 - a_2, b_1 - b_2)$ through a fixed quadratic form. Hence the metric coefficients are constant in the (a, b) chart. A two-dimensional Riemannian metric with constant coefficients is isometric (up to a linear change of variables) to a Euclidean cone, and therefore has zero curvature. \square

B. Proof of the One-Dimensional Closed Form

In this section, we prove Proposition 3.4 by deriving closed-form expressions for the orthogonal projection distance p , and the relative Wasserstein angle θ in one dimension.

Let

$$\mu = \frac{1}{n} \sum_{i=1}^n \delta_{x_i}, \quad \nu = \mathcal{N}(0, \sigma^2),$$

where $x_1 \leq \dots \leq x_n$ are sorted samples, and consider the quadratic cost $c(x, y) = \frac{1}{2} \|x - y\|^2$.

Step 1: Quantile formula for $W_2^2(\mu, \nu)$. In one dimension, the quadratic Wasserstein distance admits the quantile representation

$$W_2^2(\mu, \nu) = \int_0^1 (F_\mu^{-1}(t) - F_\nu^{-1}(t))^2 dt. \quad (6)$$

For the empirical measure μ ,

$$F_\mu^{-1}(t) = x_i \quad \text{for } t \in \left(\frac{i-1}{n}, \frac{i}{n}\right],$$

and for $\nu = \mathcal{N}(0, \sigma^2)$,

$$F_\nu^{-1}(t) = \sigma \Phi^{-1}(t),$$

where Φ denotes the CDF of $\mathcal{N}(0, 1)$.

Substituting into (6) yields

$$W_2^2(\mu, \nu) = \sum_{i=1}^n \int_{t_{i-1}}^{t_i} (x_i - \sigma \Phi^{-1}(t))^2 dt, \quad t_i = \frac{i}{n}. \quad (7)$$

Step 2: Change of variables and termwise integration. Let $t = \Phi(z)$, so that $dt = \phi(z) dz$, where ϕ is the standard Gaussian density. Define $z_i := \Phi^{-1}(i/n)$, with $z_0 = -\infty$, $z_n = +\infty$. Then

$$\int_{t_{i-1}}^{t_i} (x_i - \sigma \Phi^{-1}(t))^2 dt = \int_{z_{i-1}}^{z_i} (x_i - \sigma z)^2 \phi(z) dz.$$

Expanding and integrating termwise gives

$$\begin{aligned} \int_{z_{i-1}}^{z_i} (x_i - \sigma z)^2 \phi(z) dz &= \frac{x_i^2}{n} - 2\sigma x_i (\phi(z_{i-1}) - \phi(z_i)) \\ &\quad + \sigma^2 [-z\phi(z) + \Phi(z)]_{z_{i-1}}^{z_i}. \end{aligned}$$

Summing over $i = 1, \dots, n$ yields

$$W_2^2(\mu, \nu) = \frac{1}{n} \sum_{i=1}^n x_i^2 - 2\sigma \sum_{i=1}^n x_i (\phi(z_{i-1}) - \phi(z_i)) + \sigma^2. \quad (8)$$

Step 3: Identification of the projection length. Define the empirical scale

$$\sigma_\mu := \sqrt{\frac{1}{n} \sum_{i=1}^n x_i^2},$$

and the projection length

$$l := \sum_{i=1}^n x_i (\phi(z_{i-1}) - \phi(z_i)). \quad (9)$$

Then (8) can be written as

$$W_2^2(\mu, \mathcal{N}(0, \sigma^2)) = \sigma_\mu^2 - 2\sigma l + \sigma^2. \quad (10)$$

Step 4: Projection distance and RW_2 angle. In the cone geometry of $(\mathcal{P}_2(\mathbb{R}^d)/\sim_T, RW_2)$, the projection length l , the projection distance p , and the relative angle θ satisfy the Euclidean relations

$$l = \|[\mu]\|_{RW_2} \cos \theta, \quad \|[\mu]\|_{RW_2} = \sigma_\mu.$$

Consequently,

$$\theta = \arccos\left(\frac{l}{\sigma_\mu}\right), \quad p = \sigma_\mu \sin \theta,$$

which proves Proposition 3.4. \square

C. Closed-Form Solutions for Other Distribution Families

C.1. Closed-Form Solution for the Uniform Distribution in One Dimension

We extend the one-dimensional analysis to the family of uniform distributions and show that both the orthogonal projection distance and the relative Wasserstein angle admit explicit closed-form expressions. The derivation parallels the Gaussian case and relies on the quantile representation of the quadratic Wasserstein distance.

Let μ be a one-dimensional empirical distribution with zero mean,

$$\mu := \frac{1}{n} \sum_{i=1}^n \delta_{x_i}, \quad \bar{\mu} = 0,$$

where $x_1 \leq \dots \leq x_n$ are sorted samples. We consider the family of centered uniform distributions

$$\text{Unif}\left[-\frac{\beta}{2}, \frac{\beta}{2}\right], \quad \beta \geq 0,$$

which forms a ray in the RW_2 space.

Projection Length. Using the Euclidean structure of the filling cone, the projection length of $[\mu]$ onto the uniform ray is given by

$$\begin{aligned} l_{\text{unif}} &= \int_0^1 F_\mu^{-1}(u) \left(u - \frac{1}{2}\right) du \\ &= \sum_{i=1}^n x_i \int_{u_{i-1}}^{u_i} \left(u - \frac{1}{2}\right) du \\ &= \sum_{i=1}^n x_i \frac{2i - n - 1}{2n^2}. \end{aligned} \quad (11)$$

Importantly, l_{unif} is independent of the scale parameter β , reflecting the conic structure of the uniform family in the RW_2 space.

Relative Wasserstein Angle and Projection Distance.

The RW_2 norm of $[\mu]$ is

$$\|[\mu]\|_{RW_2} = \sigma_\mu := \sqrt{\frac{1}{n} \sum_{i=1}^n x_i^2}.$$

The relative Wasserstein angle and the orthogonal projection distance are therefore given by

$$\theta_{\text{unif}} = \arccos\left(\frac{l_{\text{unif}}}{\sigma_\mu}\right), \quad p_{\text{unif}} = \sigma_\mu \sin \theta_{\text{unif}}. \quad (12)$$

Proposition C.1 (Closed-Form Projection for the Uniform Distribution). *Let μ be a one-dimensional empirical distribution with zero mean. Then the projection length, projection distance, and relative Wasserstein angle of $[\mu]$ onto the uniform ray $[[\text{Unif}[-\beta/2, \beta/2]]]$ are given by*

$$\theta_{\text{unif}} = \arccos\left(\frac{l_{\text{unif}}}{\sigma_\mu}\right), \quad p_{\text{unif}} = \sigma_\mu \sin \theta_{\text{unif}}.$$

C.2. Closed-Form Solution for the Logistic Distribution in One Dimension

We next consider the logistic distribution, another canonical location-scale family, and derive closed-form expressions for the orthogonal projection and the relative Wasserstein angle.

Let μ be a one-dimensional empirical distribution with zero mean,

$$\mu := \frac{1}{n} \sum_{i=1}^n \delta_{x_i}, \quad \bar{\mu} = 0,$$

with sorted samples $x_1 \leq \dots \leq x_n$. We consider the family of centered logistic distributions

$$\text{Lg}(0, \sigma), \quad \sigma \geq 0,$$

which forms a ray in the RW_2 space.

Quantile Representation. The quantile function of the centered logistic distribution is

$$F_{\text{Lg}}^{-1}(u) = \sigma \psi_{\text{Lg}}(u),$$

$$\psi_{\text{Lg}}(u) = \log\left(\frac{u}{1-u}\right), \quad u \in (0, 1).$$

The empirical quantile function is again

$$F_\mu^{-1}(u) = x_i, \quad u \in (u_{i-1}, u_i].$$

Derivation of the Projection Length. The orthogonal projection length of $[\mu]$ onto the logistic ray is given by

$$l_{\text{Lg}} = \int_0^1 F_\mu^{-1}(u) \psi_{\text{Lg}}(u) du$$

$$= \sum_{i=1}^n x_i \int_{u_{i-1}}^{u_i} \log\left(\frac{u}{1-u}\right) du. \quad (13)$$

The antiderivative is explicit:

$$\int \log\left(\frac{u}{1-u}\right) du = u \log u + (1-u) \log(1-u),$$

which yields a closed-form expression for each summand in (13).

Relative Wasserstein Angle and Projection Distance.

Let

$$\|[\mu]\|_{RW_2} = \sigma_\mu := \sqrt{\frac{1}{n} \sum_{i=1}^n x_i^2}.$$

Therefore,

$$\theta_{\text{Lg}} = \arccos\left(\frac{l_{\text{Lg}}}{\sigma_\mu}\right), \quad p_{\text{Lg}} = \sigma_\mu \sin \theta_{\text{Lg}}. \quad (14)$$

C.3. Closed-Form Solution for the Laplace Distribution in One Dimension

We now consider the Laplace distribution, a canonical example of a heavy-tailed family, and derive explicit formulas for the projection distance and the relative Wasserstein angle.

Let μ be a one-dimensional empirical distribution with zero mean,

$$\mu := \frac{1}{n} \sum_{i=1}^n \delta_{x_i}, \quad \bar{\mu} = 0,$$

where the samples are sorted as $x_1 \leq \dots \leq x_n$. We consider the family of centered Laplace distributions

$$\text{Lpc}(0, b), \quad b \geq 0,$$

which forms a ray in the RW_2 space.

Quantile Representation. The quantile function of the centered Laplace distribution is given by

$$F_{\text{Lpc}}^{-1}(u) = b \psi_{\text{Lpc}}(u),$$

$$\psi_{\text{Lpc}}(u) = \begin{cases} \log(2u), & 0 < u \leq \frac{1}{2}, \\ -\log(2(1-u)), & \frac{1}{2} < u < 1. \end{cases}$$

As before, the empirical quantile function satisfies

$$F_\mu^{-1}(u) = x_i, \quad u \in (u_{i-1}, u_i], \quad u_i = \frac{i}{n}.$$

Derivation of the Projection length. Using the Euclidean structure of the filling cone, the orthogonal projection of $[\mu]$ onto the Laplace ray is given by the inner product between the quantile functions,

$$l_{\text{Lpc}} = \int_0^1 F_\mu^{-1}(u) \psi_{\text{Lpc}}(u) du$$

$$= \sum_{i=1}^n x_i \int_{u_{i-1}}^{u_i} \psi_{\text{Lpc}}(u) du. \quad (15)$$

The antiderivative of ψ_{Lpc} is explicit and piecewise:

$$\int \log(2u) du = u \log(2u) - u,$$

$$\int -\log(2(1-u)) du = (1-u) \log(2(1-u)) - (1-u).$$

Therefore, each term in (15) admits a closed-form expression depending only on the interval endpoints u_{i-1}, u_i . Importantly, the projection length l_{Lpc} is independent of the scale parameter b , reflecting the conic structure of the Laplace family in the RW_2 space.

Relative Wasserstein Angle and Projection Distance.

The RW_2 norm of $[\mu]$ is

$$\|[\mu]\|_{RW_2} = \sigma_\mu := \sqrt{\frac{1}{n} \sum_{i=1}^n x_i^2}.$$

Consequently,

$$\theta_{\text{Lpc}} = \arccos\left(\frac{l_{\text{Lpc}}}{\sigma_\mu}\right) \quad p_{\text{Lpc}} = \sigma_\mu \sin \theta_{\text{Lpc}}.$$

D. Coordinate-Separable in the PCA basis

Coordinate-separable case. Let $\bar{\mu} := \mathbb{E}_\mu[x]$ and suppose the empirical covariance of μ admits the eigendecomposition

$$\Sigma_\mu = U \text{diag}(\sigma_1^2, \dots, \sigma_d^2) U^\top,$$

where $U = [u_1, \dots, u_d]$ is an orthonormal matrix and $\sigma_k^2 > 0$. Introduce the PCA coordinates

$$y_i := U^\top(x_i - \bar{\mu}) = [y_{i,1} \quad \dots \quad y_{i,d}]^\top, \quad i = 1, \dots, n,$$

and define the one-dimensional empirical measures

$$\mu_k := \frac{1}{n} \sum_{i=1}^n \delta_{y_{i,k}}, \quad \nu_k := \mathcal{N}(0, \sigma_k^2), \quad k = 1, \dots, d.$$

We say that μ is *coordinate-separable in the PCA basis* if its equivalence class factorizes as

$$[\mu] = \bigotimes_{k=1}^d [\mu_k].$$

In this case, the quadratic cost is additive across coordinates, and the optimal transport plan between μ and any centered Gaussian with diagonal covariance in the PCA basis factorizes accordingly. As a consequence, the relative Wasserstein distance decomposes exactly as

$$RW_2^2([\mu], [\mathcal{N}(0, \Sigma_\mu)]) = \sum_{k=1}^d RW_2^2([\mu_k], [\nu_k]). \quad (16)$$

Applying the one-dimensional closed-form formula to each marginal yields

$$RW_2^2([\mu], [\mathcal{N}(0, \Sigma_\mu)]) = \sum_{k=1}^d \left[\frac{1}{n} \sum_{i=1}^n y_{i,k}^2 - 2\sigma_k \sum_{i=1}^n y_{i,k} (\phi(z_{i-1}) - \phi(z_i)) + \sigma_k^2 \right].$$

where $z_i := \Phi^{-1}(i/n)$. ϕ and Φ denote the standard normal density function and distribution function, respectively.

E. An Example Showing the Filling Cone Cannot Be Extended to Three Rays

In this section, we present an example showing that the filling-cone construction developed for two rays in the RW_2 space cannot, in general, be extended to three rays. Importantly, the obstruction is not the absence of a Euclidean isometric embedding of the three rays themselves, but rather the fact that the notion of a *filling cone* is no longer well-defined once more than two rays are involved.

Setup. Let γ denote the one-dimensional standard Gaussian distribution on the x -axis in \mathbb{R}^2 ,

$$\gamma := \mathcal{N}(0, 1) \otimes \delta_0.$$

For $\theta \in [0, 2\pi)$, let R_θ be the planar rotation by angle θ , and define

$$\mu_\theta := (R_\theta)_\# \gamma.$$

We consider the three distributions

$$\mu_1 := \mu_0, \quad \mu_2 := \mu_{\pi/3}, \quad \mu_3 := \mu_{2\pi/3},$$

corresponding to rotations by 0 , $\pi/3$, and $2\pi/3$, respectively. Each μ_i generates a ray $[[\mu_i]]$ in the quotient space $(\mathcal{P}_2(\mathbb{R}^d)/\sim_T, RW_2)$.

Pairwise filling cones. For any pair (μ_i, μ_j) , the results of Section A apply. In particular, since each μ_i is obtained from γ by a rigid rotation, the optimal transport plan between μ_i and μ_j is unique and induced by the rotation $R_{\theta_j - \theta_i}$. Consequently, the filling cone generated by the two rays $[[\mu_i]]$ and $[[\mu_j]]$ is well-defined and flat, and the corresponding RW_2 angle equals $|\theta_i - \theta_j|$.

Failure for three rays. We now explain why the filling cone cannot be consistently defined for the triple $([[\mu_1]], [[\mu_2]], [[\mu_3]])$.

Because the optimal transport plan between each pair (μ_i, μ_j) is unique, the transport maps

$$T_{1 \rightarrow 2}, \quad T_{2 \rightarrow 3}, \quad T_{1 \rightarrow 3}$$

are uniquely determined and given by rigid rotations. In particular, the quantile (or Monge) structure along the sequence

$$\mu_1 \longrightarrow \mu_2 \longrightarrow \mu_3$$

is fixed and cannot be altered.

However, if one attempts to define a three-ray filling cone by requiring that all intermediate points arise from affine combinations of the form

$$x \mapsto a x + b T_{1 \rightarrow 2}(x) + c T_{1 \rightarrow 3}(x),$$

one immediately encounters an inconsistency: the intermediate distributions generated along the pairwise filling cones (μ_1, μ_2) and (μ_2, μ_3) do not agree with those generated along (μ_1, μ_3) . In other words, there is no single family of interpolating measures whose pairwise restrictions coincide with all three uniquely determined optimal transport plans.

F. One Example where the Nearest Gaussian Does Not Share Eigenvalues or Eigenvectors

This section gives a concrete example showing that the W_2 -nearest Gaussian approximation of an empirical measure may share neither the same eigenvalues nor the same eigenvectors of the moment-matching Gaussian.

Throughout, for a finite empirical distribution $\mu = \frac{1}{n} \sum_{i=1}^n \delta_{x_i}$, we denote its mean by $\bar{\mu}$ and its empirical covariance by Σ_μ . The *moment-matching Gaussian* is $\mathcal{N}(\bar{\mu}, \Sigma_\mu)$.

F.1. A two-dimensional counterexample

Consider the empirical distribution supported on three points

$$\gamma = \frac{1}{3} (\delta_{(0,0)} + \delta_{(4,0)} + \delta_{(0,3)}),$$

with mean

$$\bar{\gamma} = \left(\frac{4}{3}, 1 \right).$$

Define the centered and RW_2 -normalized distribution

$$\mu := \frac{\gamma - \bar{\gamma}}{\|\gamma - \bar{\gamma}\|_{RW_2}},$$

so that $\bar{\mu} = 0$ and $\|\mu\|_{RW_2} = 1$.

Empirical covariance and moment matching. A direct computation shows that the empirical covariance of μ is

$$\Sigma_\mu = \frac{1}{50} \begin{pmatrix} 32 & -12 \\ -12 & 18 \end{pmatrix}.$$

which has trace one and a nonzero off-diagonal entry.

Eigenvectors: rotation angles. In two dimensions, any symmetric matrix admits an eigen-decomposition

$$\Sigma_\mu = R(\theta_{MM}) \Lambda R(\theta_{MM})^\top, \quad R(\theta) = \begin{pmatrix} \cos \theta & -\sin \theta \\ \sin \theta & \cos \theta \end{pmatrix},$$

where $\theta_{MM} \in [0, \pi)$ determines the eigenvectors. Equivalently,

$$\theta_{MM} = \frac{1}{2} \arctan \left(\frac{2\Sigma_{\mu,12}}{\Sigma_{\mu,11} - \Sigma_{\mu,22}} \right) \pmod{\pi}.$$

Substituting the entries of Σ_μ yields

$$\theta_{MM} \approx 0.8340 \pi.$$

To identify the RW_2 -nearest Gaussian direction, we perform a brute-force search over the range $\lambda \in (0, 1)$, $\theta \in [0, \pi)$,

$$\Sigma(\lambda, \theta) = R(\theta) \text{diag}(\lambda, 1 - \lambda) R(\theta)^\top,$$

which parameterizes all zero-mean Gaussian directions with unit trace. Using Monte-Carlo optimal transport combined with exact discrete OT, we obtain a minimizing Gaussian with rotation angle

$$\theta_* \approx 0.7983 \pi.$$

Since $\theta_* \neq \theta_{MM}$, the RW_2 -nearest Gaussian does not share the same eigenvectors as the moment-matching Gaussian.

Eigenvalues. The discrepancy is not limited to eigenvectors. The corresponding eigenvalues (trace one in both cases) are

$$\begin{aligned} \text{spec}(\Sigma_\mu) &= \{ 0.7778, 0.2222 \}, \\ \text{spec}(\Sigma_*) &= \{ 0.9411, 0.0589 \}. \end{aligned}$$

Thus, the RW_2 -nearest Gaussian is significantly more anisotropic than the moment-matching Gaussian, and the two Gaussians do not share the same eigenvalues.

Strict improvement in RW_2 . The associated RW_2 energies satisfy

$$\begin{aligned} W_2^2(\mu, \mathcal{N}(0, \Sigma_\mu)) &\approx 0.4865, \\ W_2^2(\mu, \mathcal{N}(0, \Sigma_*)) &\approx 0.4639. \end{aligned}$$

yielding a strictly positive gap

$$W_2^2(\text{nearest Gaussian}) < W_2^2(\text{moment-matching Gaussian})$$

of approximately 2.26×10^{-2} . This confirms that the moment-matching Gaussian does *not* lie on the nearest Gaussian ray in the RW_2 space.

Energy landscape visualization. Figure 3 visualizes the RW_2 energy landscape

$$(\lambda, \theta) \mapsto W_2^2(\mu, \mathcal{N}(0, \Sigma(\lambda, \theta)))$$

over Gaussian directions with unit trace. The moment-matching Gaussian and the RW_2 -nearest Gaussian are marked explicitly. The figure shows that the moment-matching direction is not a local minimizer of the RW_2 objective and that a different combination of eigenvalues and eigenvectors achieves a strictly smaller transport cost.

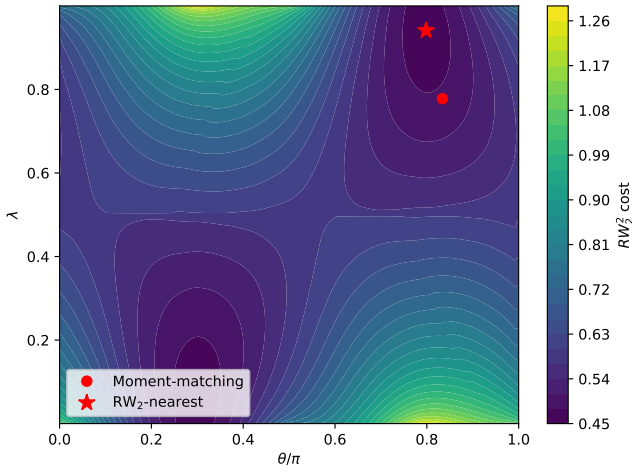


Figure 3. RW_2 energy landscape over Gaussian directions. The contour plot shows the value of $W_2^2(\mu, \mathcal{N}(0, \Sigma(\lambda, \theta)))$ as a function of the eigenvalue parameter λ and the rotation angle θ . The red dot denotes the moment-matching Gaussian, while the red star denotes the RW_2 -nearest Gaussian. The latter achieves a strictly smaller RW_2 distance, demonstrating that the moment-matching Gaussian does not lie on the nearest Gaussian ray.

Takeaway. This example provides a concrete, normalized numerical counterexample showing that, even in two dimensions and on the RW_2 unit sphere, the W_2 -nearest Gaussian approximation of an empirical distribution may share neither the eigenvectors nor the eigenvalues.

G. Relative Wasserstein Angles for Multi-Center Gaussian Mixtures

In this appendix, we illustrate the relative Wasserstein angle between empirical Gaussian mixture distributions and their nearest Gaussian approximations. The purpose of this experiment is to visualize how increasing multimodality manifests as non-Gaussianity when quantified by the RW_2 angle.

Experimental setup. We consider two-dimensional empirical distributions generated from Gaussian mixture models whose component means are arranged on a regular grid.

For a given pair (r, c) , the mixture consists of $r \times c$ Gaussian components with equal weights. Each component has isotropic covariance I , and the component means are placed on a uniform grid with fixed spacing. As r and c increase, the resulting distribution exhibits progressively stronger multimodal structure.

Nearest Gaussian and angle computation. Given an empirical sample μ , we compute its empirical covariance Σ_μ and define the reference Gaussian

$$\nu = \mathcal{N}(0, \Sigma_\mu).$$

To approximate the RW_2 distance between μ and ν , we draw Monte Carlo samples from ν and solve a discrete optimal transport problem between the empirical samples and the Gaussian samples. The resulting transport cost is then used to compute the corresponding relative Wasserstein angle.

Results. Figure 4 visualizes the empirical samples together with their associated RW_2 angles for different grid configurations. When the distribution consists of a single Gaussian component, the angle is close to zero, indicating near-Gaussian behavior. As the number of mixture components increases, the Wasserstein angle increases monotonically, reflecting a growing deviation from any single Gaussian model. This experiment demonstrates the sensitivity of the RW_2 angle to multimodality and provides an intuitive geometric interpretation of non-Gaussianity in the two-dimensional setting.

H. Stochastic Evaluation of the RW_2 Distance

In this appendix, we present the algorithm used to evaluate the RW_2 distance between an empirical distribution and a Gaussian distribution with fixed covariance. This routine forms the computational core of the high-dimensional optimization scheme.

H.1. Semi-Discrete Dual Formulation

Let

$$\mu = \frac{1}{n} \sum_{i=1}^n \delta_{x_i}, \quad \nu = \mathcal{N}(0, \Sigma),$$

where the samples $\{x_i\}_{i=1}^n$ are centered. Under the quadratic cost $c(x, y) = \frac{1}{2} \|x - y\|^2$, the semi-discrete dual formulation of the RW_2 distance is

$$\begin{aligned} RW_2(\mu, \nu) = \sup_{f \in \mathbb{R}^n} \frac{1}{n} \sum_{i=1}^n f_i \\ + \mathbb{E}_{Y \sim \nu} \left[\min_{1 \leq i \leq n} \left(\frac{1}{2} \|x_i - Y\|^2 - f_i \right) \right]. \end{aligned}$$

The dual variable $f = (f_1, \dots, f_n)$ is associated with the support points of the empirical measure.

H.2. Stochastic Dual Ascent Algorithm

Algorithm 4 Stochastic Evaluation of $RW_2(\mu, \mathcal{N}(0, \Sigma))$

Require: Samples $\{x_i\}_{i=1}^n$, covariance matrix Σ , batch size m , dual steps K_1 , stepsize η_f .

Ensure: Approximate dual potential f^* and distance estimate $RW_2(\mu, \mathcal{N}(0, \Sigma))$.

```

1: Initialize  $f^{(0)} \in \mathbb{R}^n$ 
2: for  $k = 0, \dots, K_1 - 1$  do
3:   Sample  $\xi_\ell \sim \mathcal{N}(0, I_d)$  and set  $Y_\ell = \Sigma^{1/2} \xi_\ell$ ,  $\ell = 1, \dots, m$ 
4:   for  $\ell = 1, \dots, m$  do
5:      $i_\ell \in \arg \min_i \left( \frac{1}{2} \|x_i - Y_\ell\|^2 - f_i^{(k)} \right)$ 
6:   end for
7:    $\hat{\nabla}_f L \leftarrow \frac{1}{n} \mathbf{1} - \frac{1}{m} \sum_{\ell=1}^m e_{i_\ell}$ 
8:    $f^{(k+1)} \leftarrow f^{(k)} + \eta_f \hat{\nabla}_f L$ 
9:    $f^{(k+1)} \leftarrow f^{(k+1)} - \frac{1}{n} \sum_i f_i^{(k+1)}$ 
10: end for
11: Estimate  $RW_2^2(\mu, \mathcal{N}(0, \Sigma)) \approx 2 L(f^*, \Sigma)$ 
12:
output  $f^*$ ,  $RW_2(\mu, \mathcal{N}(0, \Sigma))$ 

```

Remarks. The estimator for the dual gradient is a valid supergradient since the inner minimization is piecewise linear in f . The algorithm avoids explicit discretization of the Gaussian measure and scales well to high dimensions.

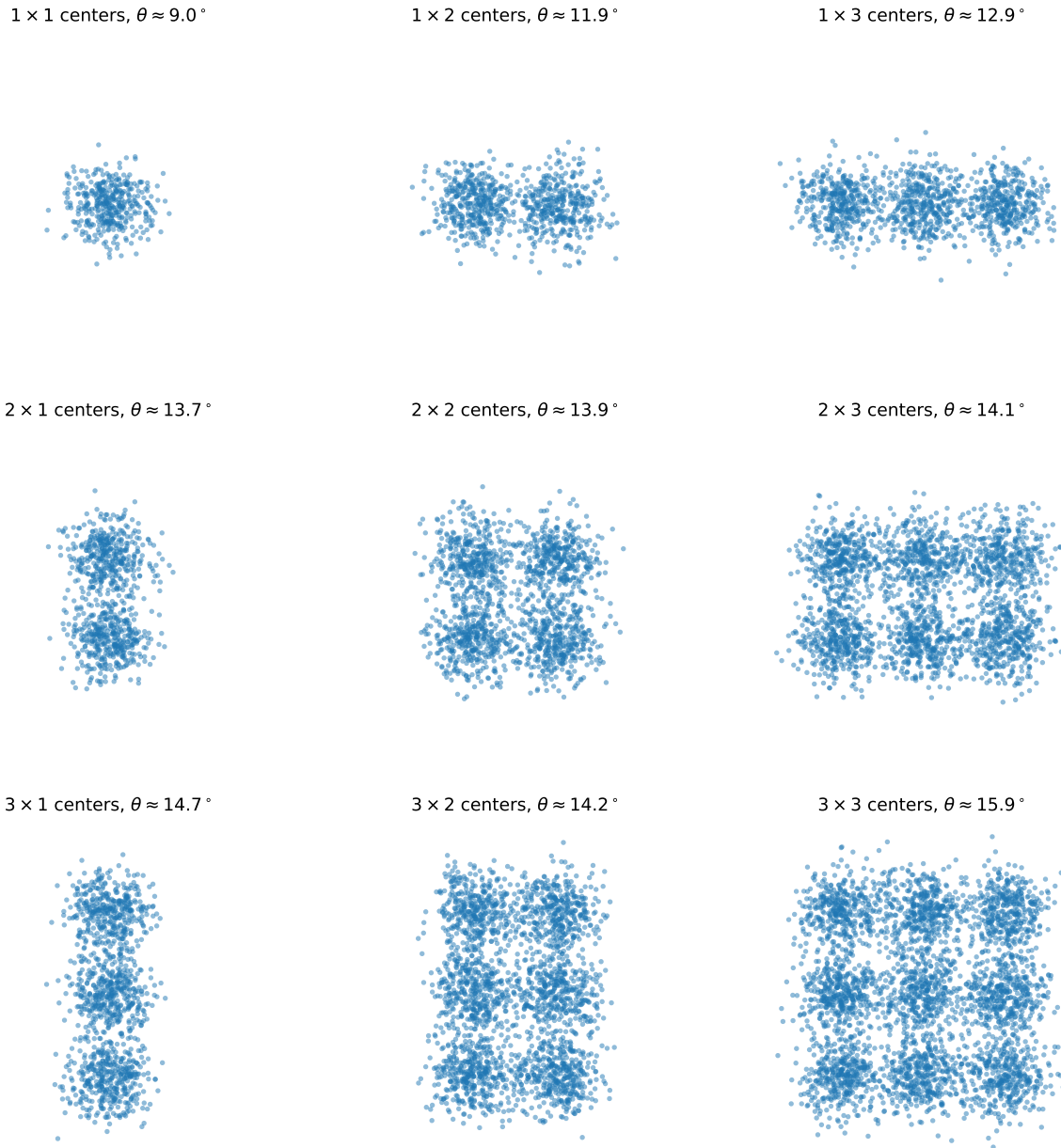


Figure 4. Relative Wasserstein angles for two-dimensional Gaussian mixture distributions with multiple centers arranged on a regular grid. Each panel shows empirical samples from a Gaussian mixture with $r \times c$ components, together with the corresponding RW_2 angle between the empirical distribution and its covariance-matching Gaussian. As the number of mixture components increases, the Wasserstein angle increases, indicating growing deviation from Gaussianity due to multimodality.